Langmuir

Article

pubs.acs.org/Langmuir

Electrochemical Nanoscale Templating: Laterally Self-Aligned Growth of Organic−Metal Nanostructures

Sohyeon Seo,[†] Tao Ye,[‡] and Eric Borguet*[,§]

[†]Department of Chemistry, Sungkyunkwan University, Suwon 440-746, Korea

[‡]School of Natural Sciences, University of California, Merced, California 95343, United States

[§]Department of Chemistry, Temple University, Philadelphia, Pennsylvania 19122, United States

Supporting Information

ABSTRACT: The electrodeposition of Ag into organized surfactant templates adsorbed onto $(22 \times \sqrt{3})$ reconstructed Au(111) is investigated by in situ electrochemical scanning tunneling microscopy. Ag^+ concentrations of as low as 2.5×10^{-6} M allow the visualization of the electrochemical molecular templating effect of a sodium dodecyl sulfate (SDS) adlayer. The SDS hemicylindrical stripes determine the adsorption sites of the Ag^+ ions and the directionality of Ag nanodeposition. The SDS-Ag nanostructures grow along the long axis of SDS hemicylindrical stripes, and an interaction of Ag with the Au(111) substrate leads to a structural change in the SDS stripe pattern. The SDS-Ag nanostructures undergo dynamic rearrangement in response to changes in the applied electrode potential. At negative potentials, the orientations of SDS-Ag nanostructures are pinned by the $(22 \times \sqrt{3})$ reconstructed pattern. Furthermore, observed differences in Ag nanostructuring on Au(111) without molecular templates (i.e., on a bare Au(111) surface) confirm the role of self-assembled organic templates in producing metal−organic nanostructures under control of the surface potential, which can determine the feature size, shape, and period of the metal nanostructure arrays.

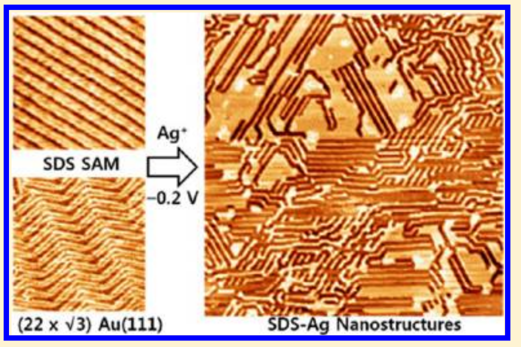

INTRODUCTION

The novel properties of metallic nanostructures make these materials attractive for a wide range of applications such as the fabrication of nanoscale devices, energy storage, catalysts, solar cells, fuel cells, and molecular electronics.[1,2] In addition to the synthesis of 1D nanoscale systems with various morphologies such as nanowires, nanotubes, and nanorods, the assembly of nanostructures into 2D or 3D arrays is necessary for the further hierarchical development of devices. Templating methods provide an interesting alternative for metal nanostructure formation.[6,7] Among the current methods, template-assisted strategies allow for both the synthesis and assembly of 1D nanostructures in one pot.[3,4] Self-organized organic templates have the potential to generate an organic−inorganic junction that is critical to the construction of molecular electronic devices.[5] Metal deposition takes place at specific sites on the template to form nanostructures such as nanofibers and nanodots.[7−12]

In principle, the molecules in self-assembled layers can determine the geometric pattern (e.g., spacings) of a molecular template and hence the sites of selective adsorption of inorganic materials to form metal−organic nanostructures.[6,13−15] Nanomaterial properties including feature size, shape, and surface assembly are determined by the chemical nature of the inorganic material and the arrangement of nanostructures.[13] Whether through the self-organization of molecule-assisted metal nanoparticle colloids[16] or metal nanopatterning through electrodeposition on the molecule prepatterned substrates,[17] the 2D organized or patterned metal nanostructures are grown under the influence of the chemical functionality of organic templates and generate an organic−metal junction.

For example, self-assembled structures of alkanes and surfactants that can form arrays of parallel 1D rows with nanometer spacings could be used as molecular templates.[18,19] Templates for nanostructure formation can be generated from the diverse structures that result from the electrode-potential-controlled self-assembly of molecules at electrified surfaces.[18] Nonetheless, the molecular-level dynamic processes that determine the potential-dependent growth of templated metal−organic nanostructures have not been reported. The structures of molecular templates formed through the self-organization of molecular building blocks are determined by both the interactions of adsorbates with the surface and the lateral interactions between adsorbates.[18,20,21] In addition, the metal percursors can also influence the adsorbed molecules and the patterns they form on the surface. Consequently, metal nanostructures on liquid−solid interfaces with molecular templates are determined by the interplay among metal−organic, intermolecular, and surface interactions.

The electrodeposition of metals and semiconductors onto surface-assembled templates is an attractive approach to the

Received: January 9, 2012
Revised: September 10, 2012
Published: December 4, 2012

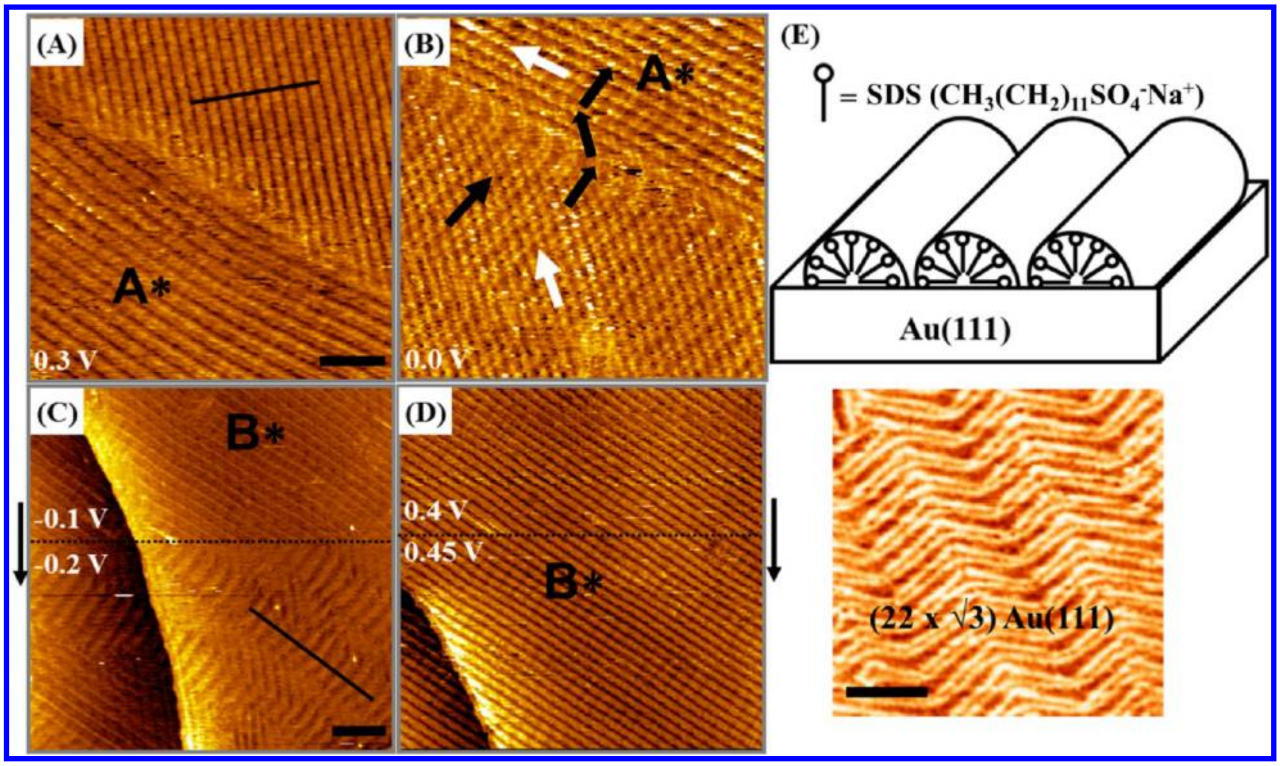

Figure 1. STM images of Au(111) as a function of potential in 0.1 M $HClO_4$ containing 10 mM SDS. (A, B) Imaged at 0.3 and 0.0 V, respectively; the black line in A marks the cross-sectional analysis, which is provided in the Supporting Information (Figure S1); white arrows in B indicate the direction of stripes of the assembled SDS molecules and the black arrow in B indicates the direction of reconstruction lines of Au(111). Scan size, 115×115 nm^2 (scale bar, 20 nm). A* indicates nearly the same area in A and B. (C, D) Effect of potential stepping on the SDS templates where the potential jumps are marked as dotted lines; the arrows along the sides of the plots indicate the scan direction. Scan size, 210×210 nm^2 (scale bar, 35 nm). B* indicates nearly the same area in C and D. (E) Cartoon representing the SDS layer on Au(111) and a typical STM image of $(22 \times \sqrt{3})$ Au(111) (image size, 60×60 nm^2; scale bar, 16 nm). A cross section of the black line in C is presented in the Supporting Information (Figure S2).

production of functional inorganic nanostructures. It has a number of advantages over traditional nanolithography, not least the possibility of parallel rather than serial processing.[22] In addition to controlled shapes and sizes, an important advantage is that these templates can prealign these as-synthesized nanostructures in 2D arrays with controlled spacing for potential nanoelectronic and nanophotonic applications, without the need for separate expensive steps (often with limited reliability) to assemble these structures after synthesis. Among a wide range of possible surface templates for electrodeposition, we have focused on physisorbed adlayers of small molecules because they potentially offer atomic-scale precision as a result of the small dimensions of preferential sites for electrodeposition.

Sodium dodecyl sulfate is known to form surface aggregates at concentrations below the critical micellar concentration. The hydrophobic chains of sodium dodecylsulfate (SDS) aggregate on surfaces to form hemicylinders, exposing the hydrophilic head groups to the aqueous environment. SDS molecules in the first surface layer lie flat to form rows with a head-to-head, tail-to-tail configuration. The unit cell of the ordered structure is 4.4 nm long and 0.5 nm wide.[23] The sulfate head groups are about 0.8 nm apart.

In a previous atomic force microscopy (AFM) study,[24] we demonstrated that Ag nanostructures are preferentially deposited onto SDS molecular templates. A key precondition for this novel preferential deposition is to reduce the Ag^+ concentration to the micromolar range, 3 orders of magnitude below that typically used for electrodepostion. Although the potential-induced structural conversion of metal nanostructures was imaged, neither the possible structural effects of the metal surface underneath metal nanostructures nor the atomic details of the metal–organic nanostructures were clearly understood because of the limited spatial resolution (ca. 2 nm) and the imaging contrast mechanism of AFM.

Herein, we have reported a high-resolution electrochemical scanning tunneling microscopy (EC-STM) study that has resolved the structures of Ag nanostructures and their relationship to the molecular template. Site-specific deposition of silver into the gaps between the hemicylinders is imaged on the submolecular/atomic level. We have identified conditions that have significantly improved the continuity of the silver wires. We have found that the electrodeposition of Ag^+ onto SDS molecular templates is affected by the interplay among Ag^+-SDS, SDS-Au(111), and Ag-Au(111) as well as the potential-induced reconstruction of Au(111). We suggest that the SDS-Ag nanostructuring process on Au(111) occurs in a series of steps: (1) the self-organization of organic molecules into a template, (2) the transformation of metal ions to organometallic precursors, and (3) the formation of metal–organic nanostructures as the applied potential changes. Our results provide an understanding of metal–organic hybrid nanostructuring on the molecular level.

■ METHODS

The Au(111) single-crystal disk (0.5 cm^2, Mateck GmbH, Germany) and Teflon STM/AFM cell (0.2 mL) were chemically cleaned with a hot piranha solution (1:3 H_2O_2 (J. T. Baker, CMOS)/H_2SO_4 (J. T.

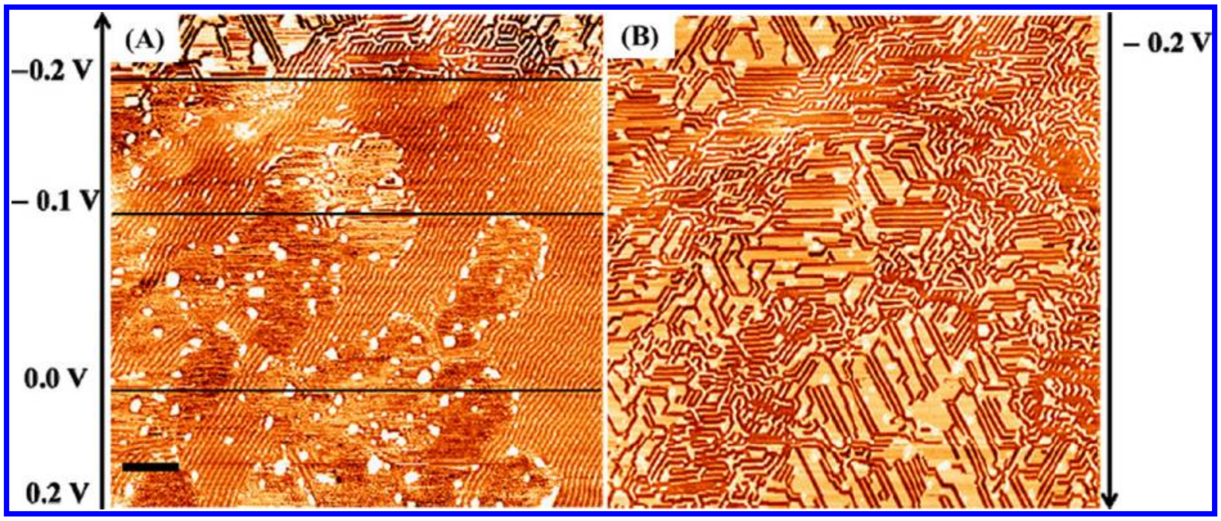

Figure 2. Ag electrodeposition on SDS/Au(111) as a function of potential in 0.1 M $HClO_4$ containing 10 mM SDS and 2.5×10^{-6} M $AgClO_4$. (A) Each potential step, from 0.2 to −0.2 V, is marked by black lines (image size, 330×330 nm^2; scale bar, 36 nm). (B) Uniform Ag nanostructures at −0.2 V after A; the arrows indicate the scan directions.

Baker, CMOS)). (***Caution!*** *Piranha solution is a very strong oxidant and is extremely dangerous to work with; gloves, goggles, and a face shield should be worn.*) The Au(111) disk was annealed by hydrogen flame before use. All solutions used in this article were prepared using purified water (18.2 MΩ·cm) (Barnstead, EasyPure with UV light). $AgClO_4$ (Aldrich, 99.999%) and SDS (Fluka, >99%) were purchased and used without further purification. STM imaging (Molecular Imaging, Picoscan 2100) was performed in 0.1 M $HClO_4$ (Fisher Scientific, Optima grade) solution under potential control provided by a bipotentiostat (Molecular Imaging, Picostat). Tungsten tips were electrochemically etched in 3 M KOH and then coated with nail polish to minimize the faradic current occurring at the tip. All STM images were recorded in constant-current mode. The electrochemical cell was composed of an Au(111) working electrode and Pt wires as the reference and counter electrodes. All potentials are quoted versus the saturated calomel electrode (SCE).

■ RESULTS AND DISCUSSION

Potential-Dependent Structures of SDS on Au(111). The SDS-covered Au(111) surface was imaged as a function of potential before Ag^+ addition in order to observe the structures formed by SDS. A striped array pattern is observed in 0.1 M $HClO_4$ containing 10 mM SDS in the potential range from 0.0 to 0.45 V (Figure 1A−C). The structure, consisting of stripes that are 4.5 ± 0.5 nm wide (Figure S1, Supporting Information), is proposed to consist of a layer of hemicylinder structures (Figure 1E) formed by SDS self-organized on the gold surface.[23,25] This long-range ordering of SDS cylindrical hemimicelles on surfaces is consistent with previous AFM[23,24] and STM[25] results. Because of the poor electrical conductivity of the alkyl chains, STM does not image the entire hemicylinder.[23] The tip likely probes the layer of SDS molecules that are in direct contact with the gold surface by temporarily displacing the molecules on the top as the STM attempts to maintain a constant current. According to the structural assignment by previous studies,[23] the dark regions correspond to the sulfate groups that point toward each other in the grooves between the cylindrical hemimicelles, and the bright regions correspond to the alkyl chains (Figure 1E).

As the substrate potential decreases from 0.3 to −0.2 V, both the reconstruction of Au(111) with its characteristic herringbone pattern[26] and the SDS-related structures are clearly resolved (Figure 1B). STM imaging of the assembly of SDS molecules at negative potentials was more difficult than at positive potentials. One possible reason is that the SDS surface assembly is destabilized at a negatively charged surface. The electrostatic repulsion between negatively charged SDS molecules and the increasingly negatively charged surface is indicated by the disappearance of the assembled SDS molecules at −0.3 V.[23,24] At −0.2 V (Figure 1C), the straight stripes associated with the SDS assembly transform into zigzag stripes that have a periodicity of ≥8.0 nm (Figure S2, Supporting Information) and therefore are distinguishable from the straight stripes observed at 0.3 V (Figure 1A) and the herringbone pattern of the Au reconstruction that are characterized by a periodicity of 6.3 nm. We take the zigzag stripes as evidence of the presence of SDS molecules on the Au surface at −0.2 V. We believe that the interaction of SDS with the Au surface weakens as the potential goes negative and that the stripe patterns (hemicylinders) of the SDS assembly deform. In the positive potential range (>0.3 V), SDS stripes were observed up to 0.45 V (Figure 1D). A potential step to 0.6 V lifted the Au(111) reconstruction to form Au islands that are characteristic of the transition from the $(22 \times \sqrt{3})$ to the (1×1) surface.[26,27] The Au islands form "landmarks" that will assist in demonstrating that metal deposition preferentially takes place between the template stripes of SDS cylindrical hemimicelles (Figures 2 and S3, Supporting Information).

Submonolayer Growth of Ag on Au(111) at Low Ag^+ Concentrations. As a control experiment for understanding the electrochemical deposition potential of Ag^+, cyclic voltammetry of bare Au(111) was performed in 0.1 M $HClO_4$ containing various Ag^+ concentrations. These experiments reveal Ag underpotential deposition (UPD) peaks (around (I) 0.9 V, (II) 0.55 V, and (III) 0.42 V) and the onset potential of the reversible or bulk deposition (around 0.38 V) at 1 mM Ag^+ concentration on bare Au(111) in 0.1 M $HClO_4$ (Figure 3). Specific chemical interactions between the metal ions and the substrate drive the underpotential process, which can lead to the formation of two UPD layers.[28] According to STM and AFM studies of Ag UPD on Au(111) at around 1 mM Ag^+ concentration, the first monolayer of Ag formed after the first UPD peak[29] (i.e., a $(\sqrt{3} \times \sqrt{3})R30$ structure), several intermediate structures were observed

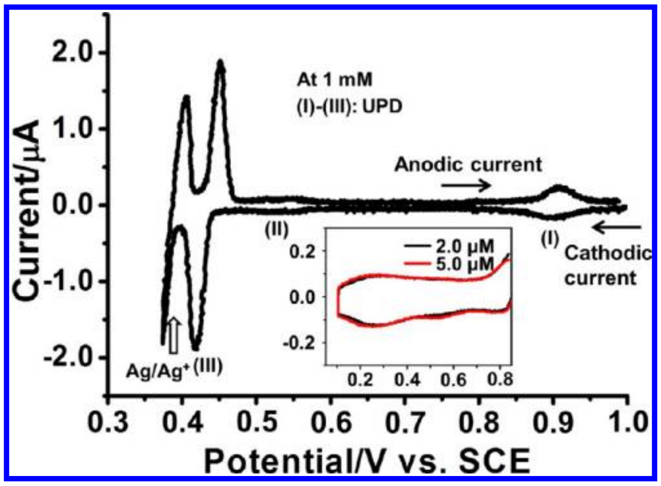

Figure 3. Cyclic voltammograms (CVs) of Au(111) in 0.1 M $HClO_4$ containing 1 mM Ag^+ at a scan rate of 10 mV s^{-1}. (Inset) CVs in 2.0×10^{-6} and 5×10^{-6} M Ag^+solutions.

between the first and second peaks (i.e., $p(n \times n)$ structures, n = 3, 4, 5, and 6), and the second monolayer of Ag formed (i.e., a (1×1)) after the third UPD peak. Bulk growth of Ag takes place via 3D growth or layer-by-layer growth on the UPD layer. As the Ag^+ concentration decreases, the Ag/Ag^+ potential shifts to the negative by 60 mV per decade according to the Nernst equation, and at 2.5×10^{-6} M solution, the bulk deposition of Ag should occur at around 0.2 V_{SCE}.[24] However, at low Ag^+ concentrations such as 5×10^{-6} M, noticeable Ag electrodeposition peaks were not observed in voltammetric measurements (inset in Figure 3). Cyclic voltammetric detection is challenging at low Ag^+ concentrations because of the diffusion limitation[24] of Ag^+ ions onto the electrode. The 0.5 cm^2 Au(111) electrode has 0.75×10^{15} atoms (given that the lattice constant a_{Au} is 2.89×10^{-10} m). The surface coverages associated with the first and second UPD monolayers are 0.25×10^{15} and 0.75×10^{15} Ag atoms, respectively. The number of Ag^+ ions (2.5×10^{-6} mol/L, 1.5×10^{18} ions/L) in a 0.2 mL STM cell is about 3×10^{15}. Consequently, the Ag^+ ions in the cell can form four layers of Ag in a layer-by-layer structure if all of the ions deposit on the surface and other factors potentially influencing the deposition process are not considered. Electrodeposition behaviors (i.e., UPD and bulk deposition, or overpotential deposition, OPD) depend on the electrode potential. However, the amount deposited (not the growth mechanism) at low concentrations is kinetically influenced by the solution phase diffusion of Ag^+. In a previous report,[24] it was found that the electrodeposition of Ag^+ was diffusion-limited at low concentrations such as 1.0×10^{-6} M. Using the Cottrell equation,[32] we determined the surface coverage of Ag to exceed 1 ML at 1 mM Ag^+ within a few minutes, and the surface coverage of Ag remained below 0.1 ML at 1×10^{-6} M on a similar time scale. In the present study, our experimental conditions lead to diffusion-limited Ag deposition.

The process of electrochemical deposition of low-concentration Ag^+ on bare Au(111) (Figure 4) and SDS/Au(111) (Figure 2) were revealed in sequential high-resolution STM images after potential steps. After the addition of Ag^+ to the SDS solution, distinct features are observed at different applied potentials. Structural changes in the SDS adlayer started at 0.2 V with the appearance of bright dots and 2D deposits (Figures 2A and S4, Supporting Information). Successive potential steps

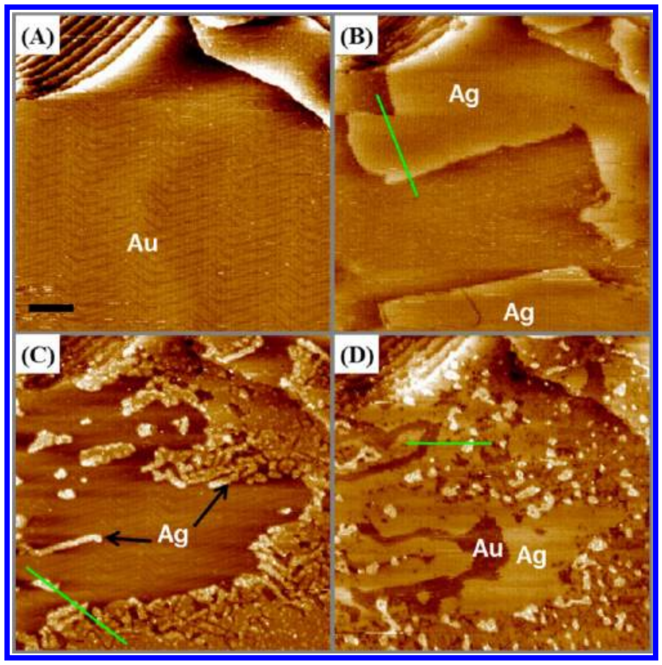

Figure 4. STM images of the $(22 \times \sqrt{3})$ reconstructed Au(111) as a function of Ag^+ concentration and potential in 0.1 M $HClO_4$. Scan size, 160×160 nm^2 (scale bar = 28 nm). (A) Imaging with no Ag^+ ions in solution at 0.2 V. (B) Imaging after the addition of Ag^+ ions (2.5×10^{-6} M $AgClO_4$) at 0.2 V; the green lines in B−D indicate the cross-sectional lines for Figure S5. (C, D) Sequentially imaged at −0.1 and +0.4 V, respectively, after the imaging in B.

to lower potentials show dramatic effects on the structure of the SDS template during Ag electrodeposition (Figure 2A). Specifically, after the addition of Ag^+ to the solution of 10 mM SDS at 0.2 V, fuzzy domains surrounding the stripes of SDS are observed. As the applied potential becomes more negative, the straight stripes become wavy, small islands appear on the wavy stripes, and finally the structure transforms into a network of 1D wires and 2D islands (or a netlike patterned layer) at −0.2 V (Figure 2B).

Ag 2D nanostructuring on the bare $(22 \times \sqrt{3})$-Au(111), which can be a template for 1D metal nanostructures,[31,33,34] is observed as a function of the electrode potential. At 0.2 V, an Au(111) surface presents a herringbone reconstruction (Figure 4A) in neat electrolyte, which confirms the presence of the reconstructed bare Au(111). While holding the potential at 0.2 V, we added Ag^+ solution to the STM cell to produce a final concentration of 2.5×10^{-6} M Ag^+. The reconstruction lines of Au(111) (Figure 4B) became blurred compared to those in Figure 4A before the addition of Ag^+. The Au(111) surface is partially covered with only a Ag^0 monolayer (Figure 4B), even though the applied potential was the Ag/Ag^+ potential. At low concentration (<0.01 mM), the electrodeposition process did not follow the expected Nernstian behavior of a 60 mV shift per decade change in the concentration[35] because the deposited metal structure may be affected by kinetic, in addition to thermodynamic, factors. Thus, the diffusion limitation of the observed processes needs to be considered at low Ag^+ concentration.

Deposited Ag is determined to be one monolayer high as shown in the cross-sectional analysis (Figure S5, Supporting Information). At the potential of Ag/Ag^+, 0.2 V in 2.5×10^{-6} M solution, a complete Ag monolayer did not form nor were multilayer structures observed, even after 20 min. This result

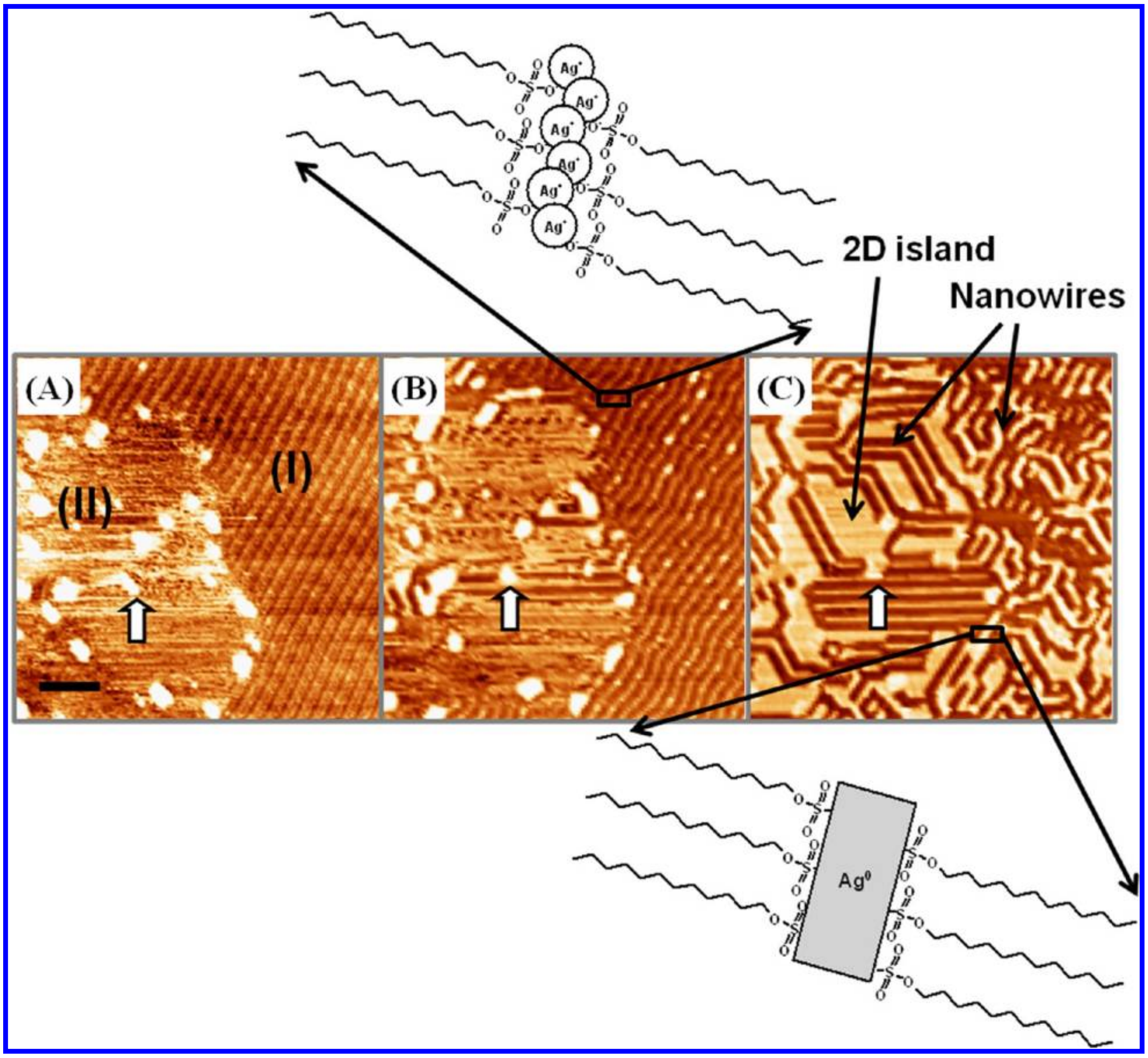

Figure 5. Sequential STM images for Ag electrodeposition on SDS/Au(111) and cartoons for proposed SDS-Ag^+/Ag^0 nanostructures in 0.1 M $HClO_4$ containing 10 mM SDS and 2.5×10^{-6} M $AgClO_4$: (A) 0.2, (B) −0.1, and (C) −0.2 V. Scan size, 100 × 100 nm^2 (scale bar, 16 nm). The white arrow indicates an island used as a landmark in successive images. (A) I and II indicate an SDS-stripe-covered region and a fuzzy region, respectively.

reveals that at this concentration Ag cannot form even a uniform monolayer, let alone multilayers or 3D structures, which is consistent with the previous report.[30] After stepping the substrate potential from 0.2 to 0.0 V (negative of the bulk deposition potential at 2.5×10^{-6} M Ag^+ solution) or even lower, the Ag^0 growth pattern changes with the appearance of small islands, two Ag atomic layers high (Figure S5, Supporting Information), indicating further epitaxial growth or structural change in the previously deposited Ag on the $(22 \times \sqrt{3})$ reconstructed Au(111)[30,31] (Figure 4C).

Potential stepping to 0.4 V (Figure 4D), which is higher than the potential of Ag/Ag^+ at 2.5×10^{-6} M Ag^+ solution, leads to the formation of a Ag^0 monolayer underneath the previous deposits formed at −0.1 V. These observations are in agreement with previous reports for Ag electrodeposition at low concentrations such as 2.0×10^{-6} M Ag^+ solution.[31] From these successive images as a function of potential, we suggest that the total extent of deposited Ag might be limited at this Ag^+ concentration and that in this regime the applied potential (between 0 and 0.4 V) controls the growth of Ag deposits to a sub- or single monolayer (lateral growth at 0.2 and 0.4 V) or to a bilayer (epitaxial growth on the monatomic layer at −0.1 V), resulting in Ag monolayers or bilayers (Figure S5, Supporting Information). Monolayer Ag^0 growth is limited to two dimensions at 0.2 V, although it is the potential of Ag/Ag^+ at 2.5×10^{-6} M Ag^+ solution. This behavior is similar to Ag UPD on Au(111).[29] Therefore, the formation of bulk deposits or a uniform monolayer would be suppressed at 0.2 V or needs more time than 20 min. Consequently, the growth of Ag nanostructures is limited to a submonolayer of Ag 2D features, one or two atomic layers high, at low Ag^+ concentrations, and the coverage of the Ag 2D nanostructures is incomplete. These behaviors of Ag electrodeposition itself on Au(111) at low concentrations can be important considerations for understanding the potential-dependent growth of nanostructures of Ag-SDS on Au(111) in Figure 2.

Laterally Self-Organized Growth of SDS-Ag Nanostructures on Au(111). To interpret the behavior of Ag electrodeposition on SDS adlayer/Au(111), STM images at each potential were carefully examined (Figures 5 and 6). An

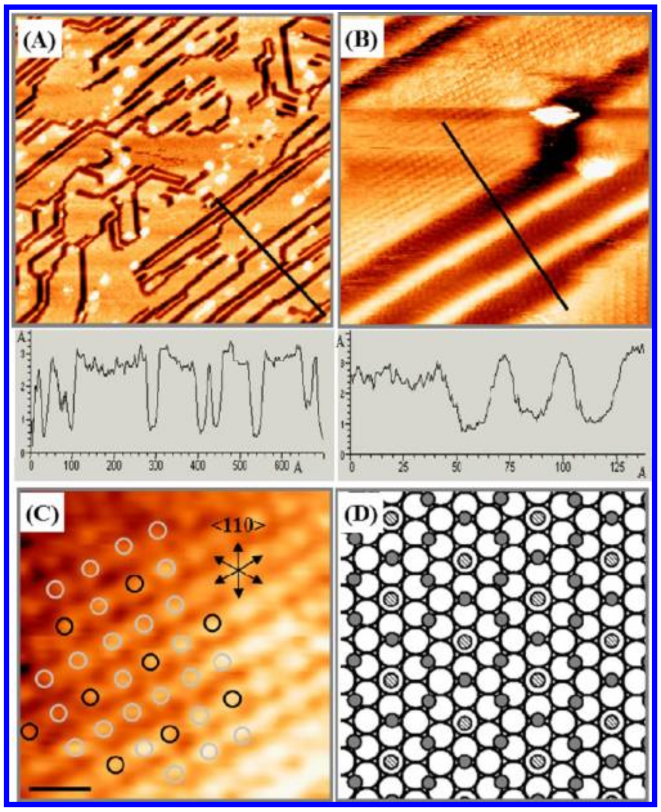

Figure 6. High-resolution STM image and cross-sectional analysis of Ag nanostructures at −0.2 V in 0.1 M $HClO_4$ containing 10 mM SDS and 2.5×10^{-6} M $AgClO_4$. Scan size: (A) 140 × 140 and (B) 19 × 19 nm^2. (C) 3.0 × 3.0 nm^2 high-resolution image of an Ag island. The black lines in A and B indicate the cross-sectional lines. (C) Arrows indicate the ⟨110⟩ directions of the Au(111) substrate that are determined by the triangular Au(111) terrace in A. Gray and black circles represent Ag atoms on different adsorption sites (scale bar, 0.6 nm). (D) Schematic of the proposed (3 × 3) lattice formed by Ag deposition on Au(111). Small circles represent Ag atoms, and large open circles represent Au atoms. Ag atoms in atop sites are black-striped circles, and Ag atoms in bridging sites are small, dark circles.

Au island was used as a landmark (indicated by an arrow in Figure 5) to follow the electrochemical templating effect of the SDS adlayer/Au(111). After adding Ag^+ solution at 0.2 V, two distinct types of regions appeared on the SDS adlayer/Au(111) surface:

(1) SDS-stripes-covered regions (region I in Figures 5A and S4) and

(2) fuzzy regions (region II in Figures 5A and S4).

Such differences could be due to the formation of Ag 2D deposits in the fuzzy domains surrounding the SDS stripes at 0.2 V where the defects (e.g., Au islands) of the SDS adlayer may serve as initial adsorption sites for Ag^+ ions. The fuzzy domains (Figure 5A,B) subsequently formed angular 2D islands at −0.2 V (Figure 5C). When the potential was stepped to −0.1 V from 0.2 V, Ag deposition apparently occurred in the region of the SDS stripes and small islands (or white dots) on wavy stripes appeared. The fuzzy domains were better resolved at −0.1 V (Figure 5B). The wavy stripes at −0.1 V become nanowires at −0.2 V (Figure 5C) in the regions of SDS stripes.

Before Ag deposition, the gaps between the SDS stripes were resolved as depressed regions in the STM images (Figure 5A). After Ag deposition, the STM images revealed Ag islands represented as bright dots on the bright wavy stripes in the gap between the SDS stripes (Figure 5B); the dark regions of the SDS stripes in Figure 5A became bright in Figure 5B. These wavy stripes on SDS/Au(111) with Ag^+ are totally different from the zigzag pattern of SDS-assembled stripes on SDS/Au(111) at −0.2 V (Figure 1C), where SDS cylindrical hemimicelles were arranged in three directions oriented 120° with respect to each other. The location of the wavy stripes was confirmed by the Au landmark in a detailed analysis of the STM images, which was in the gaps between the SDS stripes before Ag deposition (Figure S6, Supporting Information).

The STM "height" of the surface nanostructures gradually increases as they transition from straight stripes (∼0.5 Å) to wavy stripes (∼1.0 Å) and ultimately to the Ag nanowires (∼2 Å) as shown in Figure S6. Usually, a metal UPD monolayer forms because of the adsorption of ions (i.e., $Au^{\delta-}$-$Ag^{\delta+}$-counteranion).[29] Thus, the formation of $Au^{\delta-}$-$Ag^{\delta+}$-sulfate complexes (i.e., SDS-Ag^+ complexes/Au in this article) is a possible intermediate (or precursor) to SDS-Ag^0. We hypothesize that SDS-Ag^+ complexes, as precursors of Ag deposition (SDS-Ag^0), may preferentially form on the gold surface in the gaps between the SDS cylindrical hemimicelles. The wavy stripes were never observed on SDS layer/Au(111) in the absence of Ag^+ at any potential (Figure 1) or at a negative potential in Ag^+ solution. On a negatively charged substrate, the interaction between SDS molecules and the gold surface becomes weak, leading to a change from the straight stripes of assembled SDS to the wavy stripes and fuzzy domains associated with the formation of SDS-Ag^+ complexes. The wavy stripes determine the deposition sites for Ag. Thus, the SDS molecules in the cylindrical hemimicelles can form wavy stripes of SDS-Ag^+, and physically assembled SDS molecules may rearrange to straight patterns as a result of Ag deposition as SDS-Ag^0 nanostructures. At −0.2 V, the negatively charged Au(111) is electrochemically reconstructed, which leads to the formation of SDS-Ag nanostructures in short nanowires instead of long wavy nanowires presumably because of the rearrangement of the negatively charged SDS adlayer. The nanostructures are measured to be as high as a monolayer of silver (cross-sectional analysis in Figure 6A,B). The structures are uniformly oriented at 120° with respect to each other, reflecting the 3-fold symmetry of the underlying $(22 \times \sqrt{3})$-Au(111) surface. These successive images indicate that negative potentials, such as −0.1 and −0.2 V, drive a change in the interactions between the molecules and the surface, thereby changing the directionality of the Ag-SDS nanostructures.

Ag deposition appears to occur in 1D stripes (i.e., nanowires) that are 1 nm wide (fwhm) and 0.2 nm high and in 2D islands (Figure 6). In the high-resolution image of an island (Figure 6B,C), the bright spots are assigned as Ag atoms. Slightly distorted hexagonal structures are seen, and the interatomic distances are about 0.5 ± 0.04 nm. A possible structure, which satisfies the observed interatomic spacing, is a 3 × 3 lattice, where Ag atoms adsorb in atop and bridging sites of the underlying Au(111) substrate (Figure 6D).[36] For the Ag deposited area, the (3 × 3) structure of the Ag layer on Au(111) indicates 0.44 ML Ag coverage. The dark regions seem to be unoccupied with Ag deposits. Therefore, the coverage of Ag should be lower than that for a complete (1×1) Ag monolayer on Au(111). Furthermore, the nanowires and 2D islands are aligned with the long axis of the hemicylindrical stripes at −0.2 V (Figure 1) on the Au(111) surface. Ag deposition is initiated along the long axis of the SDS stripes (Figure 5B); the wavy Ag^+-SDS stripes that align with the long axis of the SDS stripes converted to Ag^0-SDS wires by changing the applied potential to −0.2 V. As a result, the alignment direction of the Ag deposits on SDS-covered Au changes to align with the Au(111) reconstruction lines at −0.2 V (Figure 5C). We believe that whereas most of the SDS molecules remained on the surface (Figure 1C) at −0.2 V some SDS molecules desorbed. As shown in Figure S6, the dark regions between the nanowires at −0.2 V corresponded to the gaps in the wavy stripes at −0.1 V and the SDS stripes at 0.2 V. In the cross section, the distances (about 4 nm) between surface structures imply the presence of SDS on the surface.

Further confirmation of the position of Ag deposits was provided by STM imaging performed in a potential range between −0.1 and 0.5 V (Figure S7, Supporting Information). The SDS array pattern on Au(111) is observed in 0.1 M $HClO_4$ containing 10 mM SDS in the potential range from 0.0 to 0.45 V (Figures 1A−C and S7A). However, the ordered SDS adlayer becomes disordered at 0.5 V (Figure S7, Supporting Information). When the potential was held at −0.1 V for over 20 min, after the addition of Ag^+, the wavy stripes appeared and became brighter (Figure S7C, Supporting Information). After the potential was stepped to 0.5 V, array patterns of white dots (presumably Ag deposits) were observed in the same regions of the wavy stripes (as marked with an arrow in Figure S7D, Supporting Information), which confirms that Ag deposition occurs in the gap between the SDS stripes. Therefore, it appears that the SDS-Ag nanostructures are formed through nucleation along the long axis of the hemicylindrical stripes that template the Ag nanostructure growth in a specific direction.

■ CONCLUSIONS

In situ electrochemical STM of Ag deposition in SDS surfactant containing electrolyte reveals lateral SDS-Ag nanostructuring on an Au(111) surface. In the absence of Ag^+ ions in solution, the straight stripes of assembled SDS molecules transform into zigzag stripes at ≤0.0 V, similar to the structure of the underlying gold herringbone pattern. In the presence of Ag^+ ions, the straight stripes of assembled SDS molecules become wavy at ≤0.2 V. A circuitlike uniform network of collective SDS-Ag nanostructures is constructed at −0.2 V, whose nanopatterns align with the directions of the underlying herringbone of the Au(111) reconstruction. Therefore, the SDS adlayer leads to the lateral self-organization of SDS-Ag nanostructures on the $(22 \times \sqrt{3})$ reconstructed Au(111) surface. The transformation of Ag nanostructures systematically occurs in the SDS adlayer/Au(111) under potential control. The electrodeposited Ag nanostructues are heavily influenced by the SDS adlayer. At the same time, the molecular template is not static and is affected by the electrode potential even after Ag^+ adsorbs on it. When we use limited metal ion concentrations, the interplay between organized surfactant templates and metal ions at the electrified surface can lead to the laterally self-aligned growth of organic−noble metal nanostructures with controlled sizes, shapes, and periodicity.

■ ASSOCIATED CONTENT

Supporting Information

STM images and cross-sectional analysis. This material is available free of charge via the Internet at http://pubs.acs.org.

■ AUTHOR INFORMATION

Corresponding Author

*E-mail: eborguet@temple.edu.

Notes

The authors declare no competing financial interest.

■ ACKNOWLEDGMENTS

We thank the National Science Foundation (CHE 0809838) for generous financial support.

■ REFERENCES

(1) Burda, C.; Chen, X.; Narayanan, R.; El-Sayed, M. A. Chemistry and Properties of Nanocrystals of Different Shapes. *Chem. Rev.* **2005**, *105*, 1025−1102.

(2) Tiano, A. L.; Koenigsmann, C.; Santulli, A. C.; Wong, S. S. Solution-Based Synthetic Strategies for One-Dimensional Metal-Containing Nanostructures. *Chem. Commun.* **2010**, *46*, 8093−8130.

(3) Qiao, Y.; Lin, Y.; Wang, Y.; Li, Z.; Huang, J. Metal-Driven Viscoelastic Wormlike Micelle in Anionic/Zwitterionic Surfactant Systems and Template-Directed Synthesis of Dendritic Silver Nanostructures. *Langmuir* **2011**, *27*, 1718−1723.

(4) Jacobs, B. W.; Houk, R. J. T.; Anstey, M. R.; House, S. D.; Robertson, I. M.; Talin, A. A.; Allendorf, M. D. Ordered Metal Nanostructure Self-Assembly Using Metal−Organic Frameworks as Templates. *Chem. Sci.* **2011**, *2*, 411−416.

(5) Chai, J.; Wang, D.; Fan, X. N.; Buriak, J. Assembly of Aligned Linear Metallic Patterns on Silicon. *Nat. Nanotechnol.* **2007**, *2*, 500−506.

(6) Kang, C.; Kim, E.; Baek, H.; Hwang, K.; Kwak, D.; Kang, Y.; Thomas, E. L. Full Color Stop Bands in Hybrid Organic/Inorganic Block Copolymer Photonic Gels by Swelling-Freezing. *J. Am. Chem. Soc.* **2009**, *131*, 7538−7539.

(7) Zhang, J.; Li, Y.; Zhang, X.; Yang, B. Colloidal Self-Assembly Meets Nanofabrication: From Two-Dimensional Colloidal Crystals to Nanostructure Arrays. *Adv. Mater.* **2010**, *22*, 4249−4269.

(8) Decker, R.; Schlickum, U.; Klappenberger, F.; Zoppellaro, G.; Klyatskaya, S.; Ruben, M.; Barth, J. V.; Brune, H. Using Metal-Organic Templates to Steer the Growth of Fe and Co Nanoclusters. *Appl. Phys. Lett.* **2008**, *93*, 243102.

(9) Fu, J.; Huang, X.; Huang, Y.; Pan, Y.; Zhu, Y.; Tang, X. Preparation of Silver Nanocables Wrapped with Highly Cross-Linked Organic-Inorganic Hybrid Polyphosphazenes via a Hard-Template Approach. *J. Phys. Chem. C* **2008**, *112*, 16840−16844.

(10) Gottlieb, D.; Morin, S. A.; Jin, S.; Raines, R. T. Self-Assembled Collagen-like Peptide Fibers as Templates for Metallic Nanowires. *J. Mater. Chem.* **2008**, *18*, 3865−3870.

(11) Guha, S.; Drew, M. G. B.; Banerjee, A. Construction of Helical Nanofibers from Self-Assembling Pseudopeptide Building Blocks: Modulating the Handedness and Breaking the Helicity. *Small* **2008**, *4*, 1993−2005.

(12) Chai, J.; Buriak, J. M. Using Cylindrical Domains of Block Copolymers to Self-Assemble and Align Metallic Nanowires. *ACS Nano* **2008**, *2*, 489−501.

(13) Jain, A.; Gutmann, J. S.; Garcia, C. B. W.; Zhang, Y.; Tate, M. W.; Gruner, S. M.; Wiesner, U. Effect of Filler Simensionality on the Order-Disorder Transition of a Model Block Copolymer Nanocomposite [5]. *Macromolecules* **2002**, *35*, 4862−4865.

(14) Simon, P. F. W.; Ulrich, R.; Spiess, H. W.; Wiesner, U. Block Copolymer-Ceramic Hybrid Materials from Organically Modified Ceramic Precursors. *Chem. Mater.* **2001**, *13*, 3464−3486.

(15) Kagan, C. R.; Mitzi, D. B.; Dimitrakopoulos, C. D. Organic-Inorganic Hybrid Materials as Semiconducting Channels in Thin- Film Field-Effect Transistors. *Science* **1999**, *286*, 945−947.
(16) Mogilevsky, A.; Jelinek, R. Gold-Nanoparticle-Self-Assembly in Two-Component Lipid Langmuir Monolayers. *Langmuir* **2011**, *27*, 1260−1268.
(17) George, A.; Maijenburg, A. W.; Nguyen, M. D.; Maas, M. G.; Blank, D. H. A.; Ten Elshof, J. E. Nanopatterning of Functional Materials by Gas Phase Pattern Deposition of Self-Assembled Molecular Thin Films in Combination with Electrodeposition. *Langmuir* **2011**, *27*, 12760−12768.
(18) He, Y.; Ye, T.; Borguet, E. The Role of Hydrophobic Chains in Self-Assembly at Electrified Interfaces: Observation of Potential-Induced Transformations of Two-Dimensional Crystals of Hexadecane by In-situ Scanning Tunneling Microscopy. *J. Phys. Chem. B* **2002**, *106*, 11264−11271.
(19) Manne, S.; Gaubt, H. E. Molecular Organization of Surfactants at Solid-Liquid Interfaces. *Science* **1995**, *270*, 1480−1482.
(20) Barth, J. V.; Weckesser, J.; Lin, N.; Dmitriev, A.; Kern, K. Supramolecular Architectures and Nanostructures at Metal Surfaces. *Appl. Phys. A: Mater. Sci. Process.* **2003**, *76*, 645−652.
(21) McNab, I. R.; Polanyi, J. C. Patterned Atomic Raction at Surfaces. *Chem. Rev.* **2006**, *106*, 4321−4354.
(22) Seo, K.; Borguet, E. Nanolithographic Write, Read, and Erase via Reversible Nanotemplated Nanostructure Electrodeposition on Alkanethiol-Modified Au(111) in an Aqueous Solution. *Langmuir* **2006**, *22*, 1388−1391.
(23) Burgess, I.; Jeffrey, C. A.; Cai, X.; Szymanski, G.; Galus, Z.; Lipkowski, J. Direct Visualization of the Potential-Controlled Transformation of Hemimicellar Aggregates of Dodecyl Sulfate into a Condensed Monolayer at the Au(111) Electrode Surface. *Langmuir* **1999**, *15*, 2607−2616.
(24) Ye, T.; Seo, K.; Borguet, E. Electrodeposition of Metal Wires onto a Molecular Scale Template: An In Situ Investigation. *Langmuir* **2009**, *25*, 5491−5495.
(25) Petri, M.; Kolb, D. M. Nanostructuring of a Sodium Dodecyl Sulfate-Covered Au(111) Electrode. *Phys. Chem. Chem. Phys.* **2002**, *4*, 1211−1216.
(26) He, Y.; Borguet, E. Dynamics of Metastable Nanoscale Island Growth and Dissolution at Electrochemical Interfaces by Time-Resolved Scanning Tunneling Microscopy. *J. Phys. Chem. B* **2001**, *105*, 3981−3986.
(27) He, Y.; Borguet, E. A Metastable Phase of the Au(111) Surface in Electrolyte Revealed by STM and Asymmetric Potential Pulse Perturbation. *J. Phys. Chem. C* **2011**, *115*, 5726−5731.
(28) Hagenström, H.; Esplandiú, M. J.; Kolb, D. M. Functionalized Self-Assembled Alkanethiol Monolayers on Au(111) Electrodes: 2. Silver Electrodeposition. *Langmuir* **2001**, *17*, 839−848.
(29) Herrero, E.; Buller, L. J.; Abruña, H. D. Underpotential Deposition at Single Crystal Surfaces of Au, Pt, Ag and Other Materials. *Chem. Rev.* **2001**, *101*, 1897−1930.
(30) Takakusagi, S.; Kitamura, K.; Uosaki, K. In Situ Real-Time Monitoring of Electrochemical Ag Deposition on a Reconstructed Au(111) Surface Studied by Scanning Tunneling Microscopy. *J. Phys. Chem. C* **2008**, *112*, 3073−3077.
(31) Takakusagi, S.; Kitamura, K.; Uosaki, K. Electrodeposition of Ag and Pd on a Reconstructed Au(111) Electrode Surface Studied by in Situ Scanning Tunneling Microscopy. *Electrochim. Acta* **2009**, *54*, 5137−5141.
(32) Bard, A. J.; Faulkner, L. R. *Electrochemical Methods: Fundamentals and Applications*; Wiley & Sons: New York, 1980.
(33) Campiglio, P.; Repain, V.; Chacon, C.; Fruchart, O.; Lagoute, J.; Girard, Y.; Rousset, S. Quasi Unidimensional Growth of Co Nanostructures on a Strained Au(111) Surface. *Surf. Sci.* **2011**, *605*, 1165−1169.
(34) Corso, M.; Fernández, L.; Schiller, F.; Ortega, J. E. Au(111)-Based Nanotemplates by Gd Alloying. *ACS Nano* **2010**, *4*, 1603−1611.
(35) Rodríguez, J. F.; Taylor, D. L.; Abruña, H. D. Concentration -Dependence of the Underpotential Deposition of Silver on Pt(111)-Electrochemical and Uhv Studies. *Electrochim. Acta* **1993**, *38*, 235−244.
(36) Chen, C. H.; Vesecky, S. M.; Gewirth, A. A. In Situ Atomic Force Microscopy of Underpotential Deposition of Ag on Au(111). *J. Am. Chem. Soc.* **1992**, *114*, 451−458.